Acta Cryst. (1979). A35, 604–610

Breakdown of Friedel's Law in the Kikuchi Patterns of Tellurium

BY G. FAIVRE AND J.-J. LE GOFF

Laboratoire des Propriétés Mécaniques et Thermodynamiques des Matériaux, Université Paris-Nord, Avenue Jean-Baptiste Clément, 93430 *Villetaneuse, France*

(*Received* 9 *October* 1978; *accepted* 2 *March* 1979)

Abstract

Evidence of the breakdown of Friedel's law in the Kikuchi patterns of tellurium crystals has been observed with a standard transmission electron microscope (TEM). These observations give a direct method of identifying enantiomorphously related phases in the TEM. An interpretation of the observed deviations from Friedel's law is proposed on the basis of the model of Thomas & Humphreys [*Phys. Status Solidi A* (1970). **3**, 599–615] for Kikuchi patterns. The possible differences between the phases of the Fourier coefficients of the crystal potential and of the absorption potential have to be taken into account. Some light is thrown on the physical significance of the phenomenological parameters.

1. Introduction

In this paper, we investigate a new method for identifying non-centrosymmetry in the structure of crystals, based upon the observation of Kikuchi patterns in a transmission electron microscope.

A large amount of work has been devoted to the problem of identifying non-centrosymmetry and enantiomorphism by electron diffraction or imaging techniques (Goodman & Lehmpfuhl, 1968; Goodman & Secomb, 1977; Van der Biest & Thomas, 1975; Steeds, Tatlock & Hampton, 1973). To reveal the lack of a center of symmetry and, *a fortiori*, to identify enantiomorphously related phases, one has to look for deviations from Friedel's law, *i.e.* for a difference between the intensity of $+\mathbf{g}$ and $-\mathbf{g}$ diffractions.

Friedel's law is a property of the equations of diffraction in the kinematical approximation and in the two-beam dynamical approximation without absorption (Laue, 1948). Only one structure factor is involved in these approximations. The breakdown of Friedel's law occurs when several structure factors with different phases are introduced to take into account either many-beam effects or anomalous absorption effects.

0567-7394/79/040604-07$01.00

In most papers that have been published on the breakdown of Friedel's law, interest is focused on many-beam effects. Absorption effects are more or less eliminated by using images or diffraction patterns from thin or very thin regions of the crystal.

The present work gives evidence of the breakdown of Friedel's law related mainly to the anomalous absorption effect. Kikuchi patterns from regions as thick as possible are used. As has been stressed by Gevers, Blank & Amelinckx (1966), in order that anomalous absorption effects can explain a deviation from Friedel's law, it is necessary to introduce into the calculation the relative phases β_g of the absorption potential. They are defined by

$$\frac{V_g'}{V_g} = \omega_g \exp i\beta_g, \tag{1}$$

V_g and V_g' being the Fourier coefficients of the crystal potential and of the absorption 'potential' respectively.

Theoretical and experimental estimations of the modulus ω_g are available in the literature ($\omega_g \simeq 0{\cdot}1$ for low-index diffractions), but almost nothing is known about the phases β_g. However, contrasts have been observed on the boundaries between domains in $BaTiO_3$ and attributed to these phases (Snykers, Serneels, Delavignette, Gevers, Van Landuyt & Amelinckx, 1977). As any value of ω_g may be, *a priori*, considered, very strong deviations from Friedel's law due to absorption effects appear possible while the deviations due to many-beam effects are always small at 100 kV.

2. Experimental results for tellurium

Our material is trigonal tellurium. The structure of this crystal is represented in Fig. 1. It belongs to one or other of the two enantiomorphously related space groups $P3_112$ (D_3^4) (right-handed screw axis, crystal *r* in Fig. 1) or $P3_212$ (D_3^6) (left-handed screw axis, crystal *l*). The high atomic number ($Z = 52$) of this element favors strong absorption effects.

The structure factors at 100 kV of the main diffractions of Te are given in Table 1. Failures of Friedel's law can appear only on Kikuchi bands of diffracting planes which are not parallel to a binary axis: all the diffractions having one of their three first indices equal to zero are thus eliminated. Only two sufficiently strong diffractions are available for our study: $11\bar{2}0$ and $11\bar{2}3$.

The crystal was oriented in the symmetrical Laue position for the diffraction investigated; photographs of the Kikuchi pattern in this orientation were taken on glass plates and several microdensitometer scans were done on each plate along directions orthogonal to the Kikuchi lines at different distances from the center of the pattern. We looked for asymmetry in the densitometer profiles. We measured the intensities I_+ and I_- of the two maxima $+g$ and $-g$ above the background intensity of the profile and calculated the asymmetry ratio

$$\Delta I/I = \tfrac{1}{2}|I_+ - I_-|/(I_+ + I_-).$$

The orientation of the crystal with respect to the incident beam is not completely determined by the condition that it is in the Laue position for the diffraction **g**. Two experimental situations can be realized depending whether the incident beam is close to or far from any low-index zone axis.

Table 1. *Structure factors of the main diffractions of* Te

g	$\lvert F_g\rvert^2$ (Å^2)
$10\bar{1}1$	407
$10\bar{1}2$	261
0003	217
$11\bar{2}0$	181
$20\bar{2}1$	116
$10\bar{1}4$	96
$20\bar{2}2$	87
$11\bar{2}3$	80

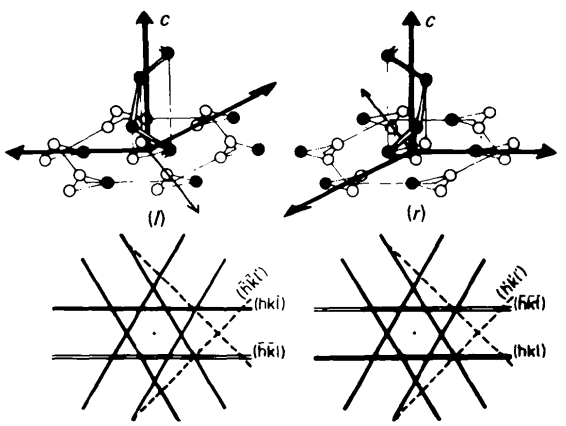

Fig. 1. Sketch of the atomic structure of two Te crystals, *l* and *r*, related by an inversion operation, and of their Kikuchi patterns (see text). *c* is the threefold helical axis. The conventional axes for hexagonal-type indexing are represented by bold lines. The same direction has indices $x_1x_2x_3$ in the *r* crystal and $\bar{x}_1\bar{x}_2x_3$ in the *l* crystal. Each diffracting plane can be given two indexings following the structure assumed for the crystal: $(hk.l)^r$ or $(\bar{h}\bar{k}.l)^l$.

2.1. *Isolated bands*

The diffraction **g** under investigation is the only strong diffraction that appears on the screen. It is then reasonable to assume that the intensity profile of the **g** band is due only to the systematic set of diffractions $n\mathbf{g}$ and to compare the experimental profile with the corresponding systematic n-beam calculation.

It appears, however, that, for both $11\bar{2}0$ and $11\bar{2}3$ diffractions, the densitometer profiles exhibit broad intensity peaks of irregular shape; the comparison with the calculated profile is not quite satisfactory. Furthermore, there is a wide dispersion among the ratios $\Delta I/I$ measured on different plates.

Several perturbations of the isolated profiles may be responsible for the dispersion of the results:

(1) The Laue position is realized with more or less accuracy ($\pm 10'$). The faces of the foil are not parallel to **g**. These two deviations from the perfectly symmetrical experimental conditions produce asymmetries in the profile which are to be considered as artefacts in the present study. However, one can make sure that these perturbations are much smaller than the effect investigated (Thomas, 1972).

(2) The background intensity is not uniform: it varies in a more or less monotonic way from one side of the plate to the other. This phenomenon is due to the irregular shape of the foil: it is related to the difficulty of preparing neat, regular, thin foils from Te crystals. The background intensity at each point of the plates has to be defined in an empirical way. An error in the measurement of $\Delta I/I$ is then obviously introduced.

(3) On each point of the band, interactions occur with Kikuchi lines of high indices. The perturbation produced on the profile of the **g** band by the line **h** depends on the ratios $|F_{h-g}/F_g|$ and $|F_h/F_g|$; it may be noticeable even if the structure factor of **h** is low. These perturbations are likely to be rather important, since the diffractions under study are not the strongest of the crystal.

We assume that all these perturbations combine to give more or less random deviations of the experimental profiles from the theoretical systematic 'isolated' profile. We thus set up for each band of a crystal an 'average experimental profile' in performing the addition of all the individual scans on the same band from one plate and from different plates corresponding to different orientations.* It appears that the average

* In doing this, we found that the ratio $\Delta I/I$ varies systematically with the distance of the scan from the center of the pattern when this distance is large enough (see §4). The results of the present section correspond to scans not too far from the center and to very thick crystals.

profiles obtained by this method have much narrower peaks than the individual profiles and agree fairly well with the calculated profiles (Figs. 2 and 3).

The dispersion among the ratios $\Delta I/I$ measured on the different average profiles is very small (Fig. 4). We therefore consider that the average profiles correspond with good precision to theoretical isolated profiles.

Two results then come out of our observations:

(*a*) the $11\bar{2}3$ band exhibits no asymmetry; $(\Delta I/I)_{11\bar{2}3} \simeq 0$,

(*b*) the $11\bar{2}0$ band exhibits a noticeable asymmetry: $(\Delta I/I)_{11\bar{2}0} \simeq 0{\cdot}15$.

2.2. *Zone axis patterns*

Fig. 5 shows the pattern obtained when the incident beam is parallel to a zone axis $\mathbf{u} = \langle 20.\bar{1}\rangle^r$ or $\langle \bar{2}0.\bar{1}\rangle^l$ for *r* or *l* crystals respectively.

The difference between the intensities of the two segments *AB* and *A'B'* of the $11\bar{2}0$ band was easily seen on the plate and is still visible on the print. It is confirmed by the densitometer scan.

Similar asymmetries can be seen on the $\langle 1\bar{1}.3\rangle$ and $\langle 00.1\rangle$ patterns, but they are much fainter (Le Goff, 1978).

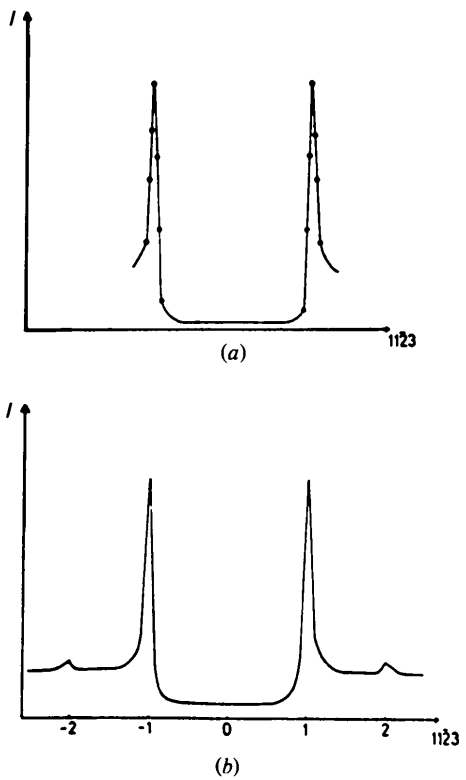

Fig. 2. Intensity profile of the $11\bar{2}3$ Kikuchi band of Te, (*a*) average experimental profile, (*b*) computed profile following the model of Thomas & Humphreys (1970) with $\beta_{ng} = 0$ for each *n*, $\omega = 0{\cdot}1$.

Near the center of the pattern, where the segments *AB* and *A'B'* lie, a large number of strong diffractions

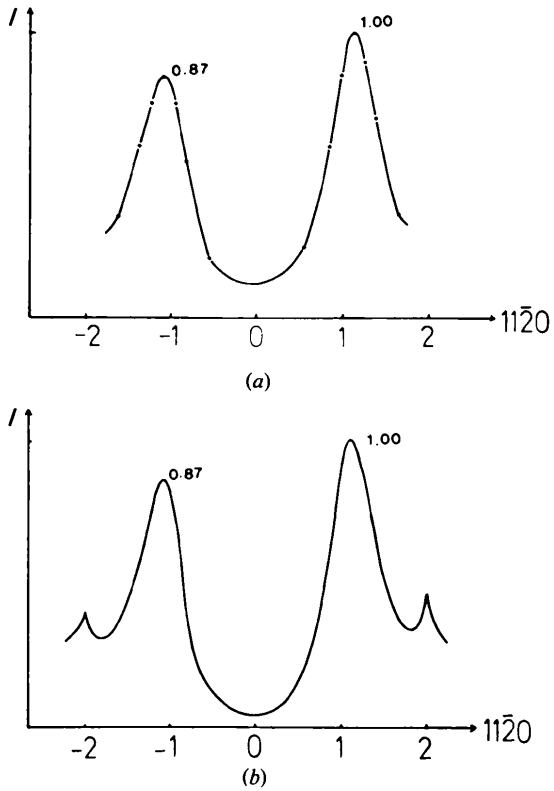

Fig. 3. Intensity profile of the $11\bar{2}0$ Kikuchi band of Te, (*a*) average experimental profile, (*b*) computed profile $\beta_g = 30°$, $\beta_{ng} = 0$ for $n > 1$, $\omega = 0{\cdot}085$.

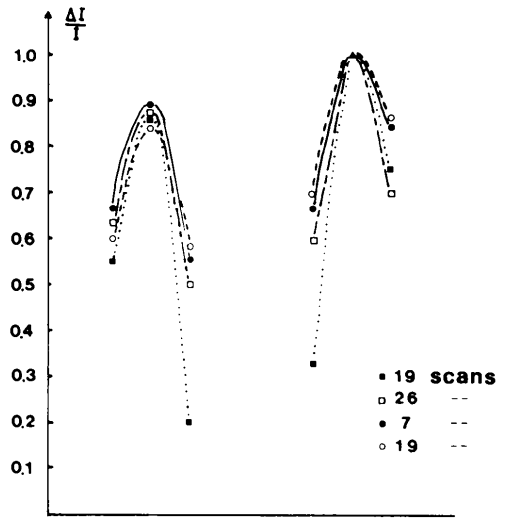

Fig. 4. Dispersion among several average experimental profiles of the $11\bar{2}0$ band, the value of the $+\mathbf{g}$ maximum being chosen as unity.

interact; many-beam effects combine with anomalous absorption effects to produce a more pronounced asymmetry than on the isolated band. However, we must examine an alternative explanation for the strong asymmetry observed in Fig. 5; it could come from interactions of the $11\bar{2}0$ band with high-order Kikuchi lines. No such line is visible in this region, but corresponding diffractions could nevertheless produce a noticeable perturbation. This last explanation can be discarded by the following procedure: on the print, we draw all the lines passing through the regions AB and $A'B'$ and we calculate their structure factors. None of them has a structure factor large enough to explain the observed effect. Another procedure which can also be used is to give a (slight) change to the accelerating voltage; the high-order lines are displaced relative to the $11\bar{2}0$ band.

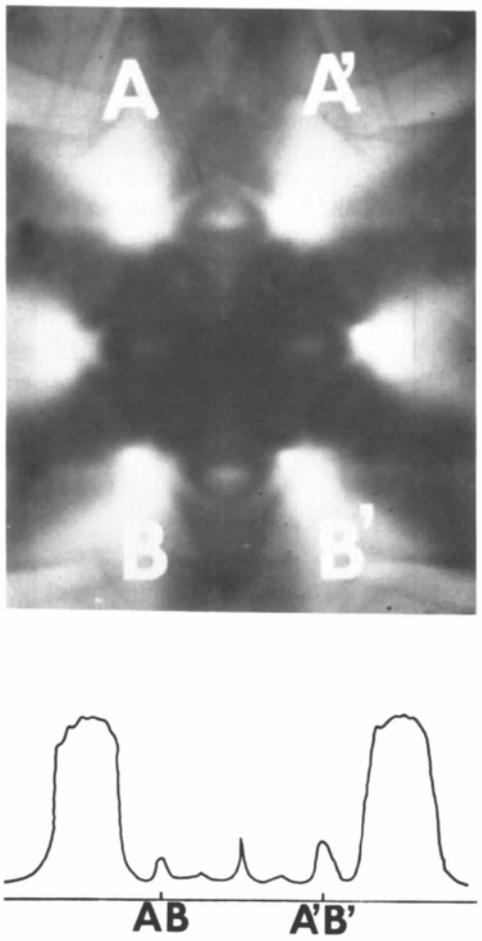

Fig. 5. $\langle 20.\bar{1}\rangle^r$ zone axis pattern of Te. The microdensitometer scan confirms the asymmetry between the intensities of the segments AB and $A'B'$ of the $11\bar{2}0$–$\bar{1}\bar{1}20$ lines. The line which has the strongest intensity on this pattern ($A'B'$) has also the strongest intensity on the isolated profiles: it can be indexed as $(11\bar{2}0)^r$ or $(\bar{1}\bar{1}20)^l$.

3. Identification of the enantiomorphously related phases

Up to now, the observations we have reported demonstrate only that crystals of Te do not belong to a centrosymmetric group. We will yet show that they allow us to identify the two phases *r* and *l* of Fig. 1.

In Fig. 1, two crystals are represented, which are related by an inversion operation: an *r* crystal and an *l* crystal in a specific orientation relation (they have the same lattice). We consider the two patterns produced by these two crystals when they are illuminated by the same incident beam parallel to a zone axis **u**. It is assumed that asymmetry is visible on the $(kk.l)^r$ or $(\bar{k}\bar{k}.l)^l$ band respectively.

The zone-axis pattern can be considered as composed of two parts or sub-patterns:

(*a*) *The 'zero-pattern'* produced by the diffractions belonging to the zero-order Laue layer (diffractions such that $\mathbf{g}.\mathbf{u} = 0$, bold lines in Fig. 1).

(*b*) *The 'non-zero-pattern'* produced by the diffractions belonging to Laue layers of order *n* greater than zero ($\mathbf{g}.\mathbf{u} = \mathbf{n} > 0$, broken lines in Fig. 1).

Reduced to the diffracting planes of the zero layer, the crystal is symmetric with respect to the plane of normal **u**; hence, applying inversion to it is equivalent to a rotation of 180° around **u**. The zero patterns of the two crystals in Fig. 1 are thus related by this rotation, or else by inversion in the plane of the pattern around its center *U*, the trace of **u** on this plane. If Friedel's law applies, or if **u** is a binary axis of the crystal, the zero pattern is symmetrical about *U*; if not, this symmetry is broken.

The non-zero pattern is not symmetrical with respect to *U*, except if **u** is a binary axis. It is not displaced by an inversion of the crystal. The lines composing this pattern are produced in the conditions where the kinematical approximation is valid; their intensity should not be significantly modified by the inversion of the crystal. The non-zero patterns are therefore identical for both *r* and *l*.

The complete patterns are thus different and can be immediately identified. By examining a crystal belonging to a known phase, one can determine once for all which pattern corresponds to which phase.

The Te single crystals out of which our thin foils were made all belonged to the dextrorotatory phase. This was determined by the etch-pits technique (Blakemore & Nomura, 1961; Ades & Champness, 1975; Koma, Takimoto & Tanaka, 1970). As expected, all the $\langle 20.\bar{1}\rangle$ patterns that we observed were identical. The pattern of Fig. 5 is thus a pattern of dextrorotatory Te.

It often happens that the non-zero pattern is not visible. Obviously, the zero-pattern alone does not allow the identification of the enantiomorphous phases, even if it exhibits a breakdown of Friedel's law; an

ambiguity remains on the orientation of the crystal. This ambiguity is easily removed by tilting the crystal. For this reason, the enantiomorphism can also be determined by noting the sense of the asymmetry of the isolated band.

4. Theoretical interpretation

We shall use the simplest model available for the interpretation of the Kikuchi patterns, the model developed by Thomas & Humphreys (1970). Following this model, Kikuchi patterns are equivalent to channelling patterns. The intensity $K(\mathbf{k})$ at a point $\mathbf{k}$ of the Kikuchi pattern is given by

$$K(\mathbf{k}) = \sum_{\mathbf{g}} I(-\mathbf{k}, -\mathbf{k}_g), \tag{2}$$

where $I(\mathbf{k}_1, \mathbf{k}_2)$ is the intensity emerging from the crystal in the $\mathbf{k}_2$ direction when it is illuminated by a beam of wave vector $\mathbf{k}_1$ and of intensity 1. In the calculation of the isolated band profile, K is a function of only one variable, the angular deviation of $\mathbf{k}$ from the Laue position and the summation in (2) is limited to the set $n\mathbf{g}$ of the systematic diffractions.

As already mentioned, the agreement between the experimental average profiles and the many-beam calculation following this model is satisfactory. However, for each of the beams taken into account, two phenomenological parameters have to be introduced into the computation: the modulus ω_{ng} and the phase difference β_{ng} defined by (1).*

It comes out from the computation that the asymmetry ratio $\Delta I/I$ depends mainly on the first parameters ω_g and β_g. An estimation based on the two-beam approximation can then be given. Following (2), one obtains easily for the intensity profile near the maximum $+\mathbf{g}$ (Gevers, Blank & Amelinckx, 1966):

$$K(w) = \cosh x + \frac{w}{(1+w^2)^{1/2}} \sinh x - 2\omega_g \sin \beta_g \frac{\sinh (2x/2)}{1+w^2}, \tag{3}$$

where $w = s_g \xi_g$ is the reduced deviation parameter for $\mathbf{g}$ diffraction and where

$$x = \omega_g \cos \beta_g \frac{2\pi}{1+w^2} \frac{t}{\xi_g}, \tag{4}$$

t being the thickness of the foil and ξ_g the extinction distance.

In our case, $t \gg \xi_g$ and $x \gg 1$. The intensity maximum occurs near the exact Bragg position $w = 0$. From (3), one obtains

$$\left|\frac{\Delta I}{I}\right| \simeq 2\omega_g \sin \beta_g. \tag{5}$$

If we take for ω_g the conventional value of 0·1, we find $|\beta_{11\bar{2}0}| \simeq 50°$.

Computations show that even when more than two beams are taken into account, the asymmetry of the $11\bar{2}0$ band can be explained only with the assumption that β_{1120} is not zero ($|\beta_{11\bar{2}0}| > 30°$). On the contrary, we find $\beta_{11\bar{2}3} \simeq 0$.

The two-beam calculation (5) leaves an indetermination in the sign of the phase $\beta_{11\bar{2}0}$. The side of the band which has the lowest intensity is the side which has a positive value of β_g. It thus appears (in Fig. 5 for example) that the determination of the sign of $\beta_{11\bar{2}0}$ and the absolute determination of the handedness of dextrorotatory Te are the same problem: either β_{1120} is positive and dextrorotatory Te is right-handed, or $\beta_{11\bar{2}0}$ is negative and dextrorotatory Te is left-handed. Since the real structure factors are easily calculated from the crystal structure, many-beam effects allow the absolute determination of the handedness. Asymmetric features related to many-beam interactions appear in the calculated profiles of the $11\bar{2}0$ band. It is therefore possible in principle to determine by the present method both the handedness of the crystal and the sign of the phases β_g. This result has not been reached yet in the case of Te because of the difficulty of ensuring reproducibility of the details of the average experimental profiles.

Discussion

The model of Thomas & Humphreys (1970), generalized for non-centrosymmetric crystals by introducing the phase β_g, gives a coherent interpretation both of the Kikuchi bands and of the deviations from Friedel's law that we have observed.

At the present time, our interpretation of the deviations from Friedel's law in the Kikuchi pattern is essentially phenomenological. Theoretical calculations of the absorption potential have been realized by several authors (see Humphreys & Hirsch, 1968; Radi, 1970); they are based on the theory of Yoshioka (1957). However, the quantity which is calculated in this theory (in addition to the fact that the computation cannot be precise) concerns 'absorption' of the purely elastically scattered electrons, whereas, in TEM, elastically and quasi-elastically scattered electrons are not separated. One remark can however be made; the theory gives no argument to support the idea that the absorption potential can be written in the same way as

* The number of independent parameters is reduced by the condition that the two potentials $V(\mathbf{r})$ and $V'(\mathbf{r})$ be real:

$$\omega_{-ng} = \omega_{ng}, \quad \beta_{-ng} = -\beta_{ng}.$$

the crystal potential as a sum over the atoms of the basis of individual spherically symmetric atomic potentials. This means that the theory does not support the simplifying assumption that the phases β_g are equal to zero.

How can we justify the evaluations given for the two phases $\beta_{11\bar{2}0}$ and $\beta_{11\bar{2}3}$ of Te? Fig. 6 gives a first phenomenological answer. The asymmetry of the Kikuchi band profile and thus the value of β_g is correlated to the asymmetry of the diffracting potential of the systematic row.

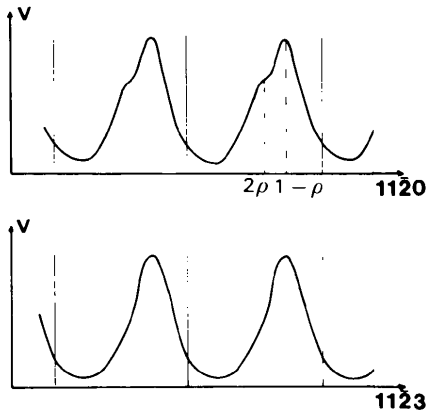

Fig. 6. Scattering potentials $V(\mathbf{r}.\mathbf{g}) = \sum_n V_{ng} \exp[2\pi i n \mathbf{g}.\mathbf{r}]$ for the two systematic rows 11$\bar{2}$0 and 11$\bar{2}$3. The maxima are located at the projections of the atoms on the row: 2ρ and $1-\rho$, where ρ is the ratio of the radius of the helical chains to the lattice parameter.

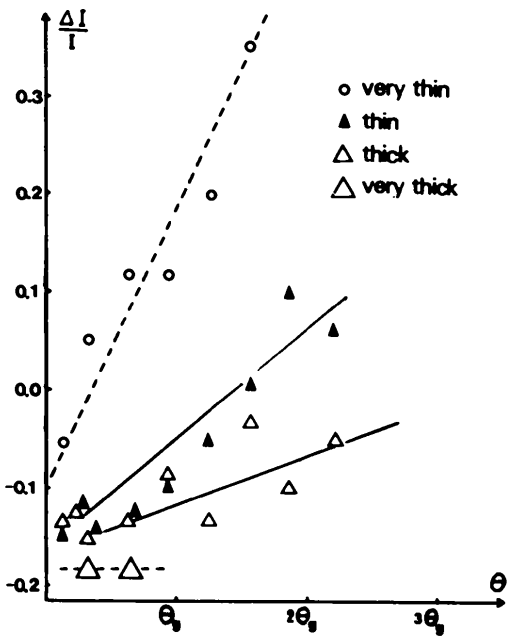

Fig. 7. Variation of the asymmetry ratio $\Delta I/I$ of the 11$\bar{2}$0 band of Te with the distance from the central line of the pattern. A series of parallel scans was made on each plate at various angular distances (θ) from the systematic row. Each point is obtained by averaging the scans corresponding to the same distance θ and to the same crystal thickness. θ_g is the Bragg angle.

The model of the equivalent divergent beam for a Kikuchi band offers an alternative interpretation of the breakdown of Friedel's law in Kikuchi patterns. In the version of Thomas & Humphreys (1970), it is assumed that the intensity distribution in the divergent beam is uniform. In the more sophisticated version of Thomas (1972), this distribution is not uniform and varies with the thickness of the crystal. In the case of a non-centrosymmetric crystal, there is no reason to eliminate the possibility that the intensity distribution itself is asymmetric even in the symmetrical Laue position. In this case, the asymmetry of the intensity profile of the Kikuchi band should vary with the thickness of the crystal.

Fig. 7 shows the value of the asymmetry ratio $(\Delta I/I)_{11\bar{2}0}$ as a function of two parameters: the thickness t of the crystal and the angular distance, θ, of the line of scanning from the central line of the pattern. Three facts are established: (1) near the central line, the dispersion is very small (see Fig. 4). $\Delta I/I$ does not vary with the thickness t if t is large enough. (2) At angular distances θ of the order of the Bragg angle, $\Delta I/I$ decreases with θ and changes its sign for larger values of θ. (3) This variation with θ is more rapid if the crystal is thin. It is negligible for the thickest crystals.

The use of the model of Thomas & Humphreys seems thus to be completely justified near the center of the Kikuchi pattern of the thickest crystals.

On the other hand, the inversion of the asymmetry far from the center of the diagram cannot be explained with this model, even in the more complete version given by Thomas. It probably indicates a fundamental shortcoming of the model, as does the well known phenomenon of contrast inversion of Kikuchi bands (Thomas, 1972). It is hoped that systematic measurements of the asymmetry ratio of the Kikuchi bands of non-centrosymmetric crystals as a function of various physical parameters will give some valuable new information on the mechanism of the formation of Kikuchi patterns.

References

ADES, S. & CHAMPNESS, C. H. (1975). *J. Opt. Soc. Am.* **65**, 217–218.

BLAKEMORE, J. S. & NOMURA, K. C. (1961). *J. Appl. Phys.* **32**, 745–746.

GEVERS, R., BLANK, H. & AMELINCKX, S. (1966). *Phys. Status Solidi*, **13**, 449–465.

GOODMAN, P. & LEHMPFUHL, G. (1968). *Acta Cryst.* A**24**, 339–347.

GOODMAN, P. & SECOMB, T. W. (1977). *Acta Cryst.* A**33**, 126–133.

HUMPHREYS, C. J. & HIRSCH, P. B. (1968). *Philos. Mag.* **18**, 115–122.

KOMA, A., TAKIMOTO, E. & TANAKA, S. (1970). *Phys. Status Solidi*, **40**, 239–248.

LAUE, M. VON (1948). *Röntgenstrahlinterferezen*. Leipzig: Akademische Verlag.

LE GOFF, J. J. (1978). Thèse de 3ème cycle, Univ. Paris XIII.

RADI, G. (1970). *Acta Cryst.* A**26**, 41–56.

SNYKERS, M., SERNEELS, R., DELAVIGNETTE, P., GEVERS, R., VAN LANDUYT, J. & AMELINCKX, S. (1977). *Phys. Status Solidi A*, **41**, 51–63.

STEEDS, J. W., TATLOCK, G. J. & HAMPTON, J. (1973). *Nature (London)*, **241**, 435–439.

THOMAS, L. E. (1972). *Philos. Mag.* **26**, 1447–1465.

THOMAS, L. E. & HUMPHREYS, C. J. (1970). *Phys. Status Solidi A*, **3**, 599–615.

VAN DER BIEST, O. & THOMAS, G. (1977). *Acta Cryst.* A**33**, 618–621.

YOSHIOKA, M. (1957). *J. Phys. Soc. Jpn*, **12**, 618–628.

Acta Cryst. (1979). A**35**, 610–613

On the Contributions of the Internal Modes of Molecules to the Debye–Waller Factors. II. Theoretical Considerations

BY C. SCHERINGER

*Institut für Mineralogie der Universität Marburg, D*3550 *Marburg, Federal Republic of Germany*

AND A. FADINI

Institut für Anorganische Chemie der Universität Tübingen, D 7400 *Tübingen, Federal Republic of Germany*

(*Received* 2 *January* 1979; *accepted* 12 *February* 1979)

Abstract

It is shown that the expressions for the contributions of the internal modes of molecules to the Debye–Waller factors as derived, on the one hand, by means of lattice dynamics and, on the other hand, by means of the **FG** method common in spectroscopy, are identical after some approximations have been made in the lattice dynamical formulation. It is pointed out that for those methods of establishing the force constant matrix of the internal modes, where the eigenvalues of the **FG** matrix are constrained to be the squares of the observed frequencies, only standard eigenvector routines need be applied in determining the mean-square-amplitude matrix. Hence, in this case, series expansions which were suggested to circumvent the determination of eigenvalues are superfluous.

1. Introduction

The calculation of the contributions of the internal modes of molecules to the Debye–Waller factors should follow a theory of the crystal (lattice dynamics), but, as a rule, crystallographers adopt the **FG** method which was established in spectroscopy and refers to isolated molecules. If one starts from the equations of lattice dynamics and eliminates the typical (intermolecular) crystal effects, the equations of lattice dynamics should become equivalent with those of the **FG** matrix formalism. This equivalence, which is not obvious, will be proved in this paper.

In a further part of the paper, we show how the formalism of the **FG** method can be simplified by introducing standard eigenvector routines. The mean-square-amplitude matrix of the internal modes of the molecules then can often be obtained in a simple fashion, and the series expansions proposed (Cyvin, 1968; Øystein, 1972) are superfluous.

2. The lattice dynamical approach

Here we make use of the description which was developed in earlier work (Scheringer, 1972*a*,*b*). The $3n \times 3n$ mean-square-amplitude matrix **U** of the n atoms in the unit cell is given by

$$\mathbf{U} = N^{-1}\mathbf{Q}\sum_{\mathbf{q}}(\mathbf{R}\mathbf{\Lambda}^{-1}\mathbf{\Gamma}\tilde{\mathbf{R}})_{\mathbf{q}}\mathbf{Q}^{T}. \quad (1)$$

The superscript T denotes the transposed matrix, -1 the inverse, and $\sim$ the conjugate complex transposed matrix. N is the number of cells in the crystal, **Q** a $3n \times 3n$ diagonal matrix, with the 3 elements $m_r^{-1/2}$ for the rth atom (m_r = mass). $\mathbf{\Lambda}(\mathbf{q})$ is a $3n \times 3n$ diagonal matrix containing, as elements, the squares of the frequencies $\omega_j(\mathbf{q})$. **q** denotes a wave vector of the

0567-7394/79/040610-04$01.00